

**NASA TECHNICAL  
MEMORANDUM**



**NASA TM X-1140**

**NASA TM X-1140**

FACILITY FORM 602	N65-34438	_____
	(ACCESSION NUMBER)	(THRU)
	29	_____
	(PAGES)	(CODE)
_____	_____	24
(NASA CR OR TMX OR AD NUMBER)	_____	(CATEGORY)

**MEASUREMENTS OF BREMSSTRAHLUNG  
PRODUCED BY 0.75 AND 1.25 MEV  
ELECTRONS INCIDENT ON TYPICAL  
APOLLO WALL SECTIONS**

*by H. D. Hendricks, T. G. James  
Langley Research Center  
Langley Station, Hampton, Va.  
and Larry B. York  
Manned Spacecraft Center  
Houston, Texas*

GPO PRICE \$ \_\_\_\_\_

CFSTI PRICE(S) \$ \_\_\_\_\_

Hard copy (HC) \_\_\_\_\_

Microfiche (MF) \_\_\_\_\_

ff 653 July 65

MEASUREMENTS OF BREMSSTRAHLUNG PRODUCED BY  
0.75 AND 1.25 MEV ELECTRONS INCIDENT  
ON TYPICAL APOLLO WALL SECTIONS

By Herbert D. Hendricks, Thomas G. James

Langley Research Center  
Langley Station, Hampton, Va.

and

Larry B. York

Manned Spacecraft Center  
Houston, Texas

NATIONAL AERONAUTICS AND SPACE ADMINISTRATION

MEASUREMENTS OF BREMSSTRAHLUNG PRODUCED BY  
0.75 AND 1.25 MEV ELECTRONS INCIDENT  
ON TYPICAL APOLLO WALL SECTIONS

By Herbert D. Hendricks, Thomas G. James  
Langley Research Center

and Larry B. York  
Manned Spacecraft Center

SUMMARY

Typical Apollo wall sections were irradiated with 0.75 and 1.25 Mev electrons from an electron accelerator. The intensity and angular distribution of the bremsstrahlung produced in and attenuated by the wall sections were measured.


The maximum dose rates are received through the thinnest wall sections. The maximum dose rate and bremsstrahlung intensity from all wall sections are always greatest in the direction of the electron beam and decreases sharply on each side of the beam. Bremsstrahlung spectra show a maximum photon intensity at energies between 80 and 115 Kev and a greater intensity of high-energy bremsstrahlung photons from 1.25 Mev electrons than from 0.75 Mev electrons.

INTRODUCTION

Development flights of the Apollo spacecraft at orbital altitudes of less than 300 miles are being considered. During these flights personnel on board will be exposed to bremsstrahlung caused by radiation-belt electrons (refs. 1 to 6). The walls of the Apollo spacecraft are composite structures and experimental measurements are required to substantiate theoretical bremsstrahlung dose rates for this type of material. The present experimental investigation was initiated upon request of the Manned Spacecraft Center. Experimental data on the bremsstrahlung produced within and transmitted through the composite wall structure were needed in order to supply the contractors with experimental data for comparison with their calculations. The present paper covers only the experimental portions of this program.

In this investigation bremsstrahlung was produced by irradiating Apollo wall sections with 0.75 and 1.25 Mev electrons. Spectra and dose rates from bremsstrahlung were measured and are presented.

34438



## APPARATUS, WALL SECTIONS, AND TESTS

### Electron Accelerator

A cascaded rectifier type of electron accelerator was used in the present investigation. This accelerator is capable of producing electrons with an energy range from 30 Kev to 1.25 Mev. A full description of this type of accelerator can be found in reference 7.

### Wall Sections

Description.- Four typical Apollo wall sections were used in this study. Wall sections A, C, and D consisted of an outer honeycomb reinforced ablation material, a structural section of stainless-steel honeycomb, an insulation blanket, and an inner structural section of aluminum honeycomb; whereas, section B consisted only of ablation material and stainless-steel honeycomb. Photographs of the wall materials are shown as figure 1. An end view of the honeycomb reinforced ablation material is also shown in figure 1(f). Wall section A is typical of the wall in the forward compartment of the spacecraft. Wall section B is typical of the wall in the vicinity of the window. Wall section C is typical of the wall in the bottom compartment. Wall section D is similar to wall section A but has a different ablation material.

Properties of the wall sections are listed in table I. The composition of the ablation materials for wall sections A, B, and C of the Apollo spacecraft, as obtained from the manufacturer, is presented in table I(a). The composition of wall section D is also given in table I(a). The effective atomic numbers of sections A, B, C (8.35), and D (8.87) were calculated by the method described in reference 4. The density given for the ablation material of sections A, B, and C was  $0.56 \text{ g/cm}^3$ . The density given for the ablation material of section D was  $0.92 \text{ g/cm}^3$ . The physical properties and structural arrangements of wall sections A, B, C, and D are given in table I(b) and figure 2, respectively. It is to be noted that section D ablation material is different from the materials of sections A, B, and C. For all wall sections the thickness of the ablation material alone is in excess of the electron energies used in this investigation.

Mounting.- The wall sections were mounted separately on the target chamber of the accelerator as shown in figure 3. The ablation material was mounted inside a sample mounting flange so that it would be inside the accelerator vacuum chamber. This type of mounting allowed the ablation material to receive the full beam of electrons from the accelerator. A vacuum seal was made at the sample flange with the stainless-steel honeycomb faceplate. The insulation blanket and the aluminum honeycomb were held in contact with the other sections by a sample clamp. This type of mounting to the accelerator chamber allowed all tests to be made with a vacuum, inside the chamber, of less than  $10^{-5}$  torr. The Faraday cup used to measure the electron beam current and the beam aperture is also shown in figure 3.

Flanges to orient a sample at a beam incidence angle of  $90^\circ$ ,  $60^\circ$ , and  $45^\circ$  (in the horizontal plane) with respect to the beam were attached to the accelerator chamber in the same position as the sample mounting flange (fig. 3). The accelerator target chamber with wall section C mounted at a beam incidence angle of  $45^\circ$  is shown in figure 4.

### Test Procedure

When a wall section was mounted at a given beam incidence angle and a detector located at a given detector angle (fig. 5), the wall section was ready to be irradiated. However, prior to any test at a particular test energy (0.75 or 1.25 Mev) the accelerator output was monitored for any current due to field emission from the dynodes of the accelerator. If this current, usually referred to as cold discharge, is greater than a few tenths of a percent of the beam current to be applied to the test wall section, the accelerator is adjusted to a higher energy. If the accelerator is operated at this higher energy, the cold discharge current decreases to an acceptable value. After the foregoing procedure the accelerator is adjusted to the test energy. The beam current was then turned on and adjusted to its proper value by measuring the current impinging on the Faraday cup (fig. 3). After the current was adjusted, the Faraday cup was rotated out of the beam and the beam could then impinge upon the ablation material. Any drift of the beam position was detected by monitoring current pickup on the beam aperture plate (fig. 3).

When the electron beam current had been adjusted to the correct value, at an electron energy of 0.75 or 1.25 Mev, a 10-minute measurement of the bremsstrahlung spectra was taken or a dose-rate measurement was made at a given detector angle. Then the Faraday cup was rotated back into the beam and the beam current was checked. If the beam current was not within 2 percent of the initial value, the data were discarded and the measurement was repeated. If the beam current was within 2 percent of the initial value, the detector was moved to another angle and the foregoing procedure was repeated.

## MEASUREMENTS AND ACCURACY

### Beam Energy

The beam energy of the accelerator used in this investigation was previously determined by finding the end-point energy for the transmission of electrons through aluminum foils. The results from this technique indicate that the beam energy is within  $\pm 2$  percent of the nominal value stated.

### Beam Current

Beam current was measured by rotating the Faraday cup (fig. 3) into the electron beam. The resulting current picked up by the Faraday cup was measured with an electrometer (accuracy of 1 percent). Prior to the experiment, a check of the beam current stability was made for a period of 10 minutes at various



beam currents. Measurements of beam currents at 25, 50, 100, and 250 nA revealed a drift of less than 2 percent.

Prior to the experiment, a check of the size of the electron beam was made. This test was performed with polyvinyl chloride film, which darkens under irradiation, and revealed a total beam cross section of approximately 2.42 sq cm at 0.75 Mev and 1.55 sq cm at 1.25 Mev.

#### Bremsstrahlung Dose Rate

The wall section to be irradiated, at an electron energy of either 0.75 or 1.25 Mev, was mounted on the accelerator target chamber at a beam incidence angle of 90°, 60°, or 45°. The ionization chamber was then fixed at a detector angle of either 0°, 15°, 30°, 45°, or 60°, as shown in figure 5. The wall section was then irradiated at a given beam incidence angle and the dose rate was measured at the various detector angles. At the detector angle of 60° the physical extent of the wall section was too small to insure that all the bremsstrahlung passed through the entire wall section. As a result of the lessened attenuation, the dose rate measured at 60° will be slightly too large. The detector angle was within  $\pm 2^\circ$  of the angles indicated in figure 5. Only wall section C was irradiated at beam incidence angles of 60° and 45°. Beam currents of 25, 50, 100, and 250 nA were used to obtain dose-rate measurements. The dose rates obtained during the tests varied linearly with beam current intensity. Consequently, the dose rates given herein were obtained from normalizing the dose rates from the four beam currents to a dose rate at 100 nA and then averaging the four resulting dose rates.

An air ionization chamber having a 500-cc sensitive volume was used to measure the bremsstrahlung dose rates. Calibration of the ionization chamber was checked before and after each test with a 16-milliroentgen (mR) source. Drift was noted to be less than  $\pm 1$  mR per hour. The dose rate from the ionization chamber is linear within  $\pm 5$  percent for gamma or X-rays of 10 Kev to 2.0 Mev. It is estimated that the normalized dose rates are within  $\pm 10$  percent of their true values. Measurements to determine any background with the accelerator on and no beam current indicated no measurable background.

#### Bremsstrahlung Spectra

The wall section to be irradiated, at an electron energy of either 0.75 or 1.25 Mev, was mounted on the accelerator target chamber at a beam incidence angle of either 90°, 60°, or 45°. A NaI(Tl) scintillation detector and a preamplifier were then fixed at a detector angle of either 0°, 15°, 30°, 45°, or 60°, as shown in figure 5. The wall section was then irradiated at a given beam incidence angle and the bremsstrahlung spectra measured at the various detector angles. The detector angles were located within  $\pm 2^\circ$  of the angles shown in figure 5. Bremsstrahlung spectra measurements were taken for the same beam incidence and detector angles as were used in obtaining the dose rates given in table II.

All bremsstrahlung spectra were taken with a beam current of  $25 \pm 0.5$  nA. The bremsstrahlung spectra measurements were made by using a  $1\frac{1}{4}$ -in. by 1-in. cylindrical NaI(Tl) scintillation crystal and preamplifier in conjunction with a single channel pulse-height analyzer (ref. 8). A lead cylinder 3 inches in diameter and 4 inches long with a 1/2-inch-diameter opening was used to collimate the bremsstrahlung and to reduce the bremsstrahlung to levels which would not cause hysteresis in the crystal. The detector and pulse-height analyzer were calibrated for 1 Mev full-scale reading. The 0.662 Mev gamma rays from a 0.5 microcurie Cs<sup>137</sup> source were used as a reference in the calibration. A window width of 5 Kev was used. The resolution of the entire pulse-height analyzer and detector system for 0.662 Mev gamma rays from Cs<sup>137</sup> was approximately 11 percent. A 0.5 microcurie Ba<sup>133</sup> gamma source with gamma rays of 0.355 and 0.082 Mev was used to check the linearity of the detector and pulse-height analyzer. The calibration of the system was checked before and after each bremsstrahlung spectrum was taken. Reproducibility of the detector and pulse-height analyzer was approximately  $\pm 5$  Kev. Measurements with the accelerator on and no beam current indicated that the background was insignificant.

The total detection efficiency, shown in figure 6, was calculated by a computer method (refs. 9, 10, and 11) for the  $1\frac{1}{4}$ -in. by 1-in. cylindrical NaI(Tl) scintillation crystal. These data are presented as an aid in interpreting the bremsstrahlung spectra.

## RESULTS AND DISCUSSION

### Bremsstrahlung Dose Rates

The dose rates from the bremsstrahlung produced in and attenuated by the Apollo wall sections in this investigation are listed in table II. The dose rates are given as a function of beam incidence angle, detector angle, and electron energy. For a beam incidence angle of  $90^\circ$ , a detector angle of  $0^\circ$ , and an electron energy of 1.25 Mev, a comparison of the bremsstrahlung production and attenuation in the different wall sections can be made. An examination of the normalized dose rate under these conditions indicates that, in general, the greater the wall shielding thickness ( $\text{g}/\text{cm}^2$ ) the lower the dose rate. Section B has the smallest wall shielding thickness ( $1.411 \text{ g}/\text{cm}^2$ ) and the highest dose rate. Section C has the largest wall shielding thickness ( $4.535 \text{ g}/\text{cm}^2$ ) and the lowest dose rate. Sections A and D have wall shielding thicknesses of  $2.143$  and  $2.181 \text{ g}/\text{cm}^2$ , respectively, and dose rates between those of sections B and C. The observed dose rates for sections A and D do not follow as closely as their wall thicknesses. However, the observed values fall within the accuracy of the investigation. For 0.75 Mev electrons incident on the sections with the same conditions as discussed previously, the same general trend can be seen from the dose rates given in table II. The bremsstrahlung dose rates received from 0.75 Mev electrons was substantially less than the dose rates received from 1.25 Mev electrons.

With 0.75 or 1.25 Mev electrons incident on the sections, it can easily be seen that, as the detector angle increases, the measured dose rate decreases. This phenomenon is verified by the data listed for section D as the detector angle increases from  $0^\circ$  to  $60^\circ$ .

During three measurements on section C, with an electron energy of 1.25 Mev, the beam incidence angle was set at  $90^\circ$ ,  $60^\circ$ , and  $45^\circ$ . It can be seen in table II that there is a decrease in dose rate with a decrease in beam incidence angle. The significance of this decrease in dose rate with an increase in detector angle or a decrease in beam incidence angle is that the emission of bremsstrahlung is predominately in the direction of the incident electron beam.

### Bremsstrahlung Spectra Measurements

The bremsstrahlung spectra presented in figures 7 to 15 show the intensity (counts/min) of bremsstrahlung as a function of energy for various beam incidence and detector angles. The maximum bremsstrahlung intensity (counts/min) for all sections under all test conditions occurs at photon energies between 80 and 115 Kev. The maximum bremsstrahlung intensity does not occur at any significantly different energy for the 0.75 Mev electrons than it does for the 1.25 Mev electrons. For all wall sections there is a greater intensity of high-energy bremsstrahlung photons from incident 1.25 Mev electrons than from incident 0.75 Mev electrons. The general shape of these bremsstrahlung spectra is typical of the shapes of bremsstrahlung spectra from previous investigations (refs. 12 to 15) using other target materials. For a beam incidence angle of  $90^\circ$ , a detector angle of  $0^\circ$ , and an electron energy of 1.25 Mev, a comparison of the bremsstrahlung spectra for the different wall sections can be made. In general, the results indicate that sections A, B, and C follow the trend of lower intensity for walls of greater shielding thickness ( $\text{g/cm}^2$ ). The same trend holds true when 0.75 Mev electrons are incident upon sections A, B, and C. There is a greater intensity of high-energy bremsstrahlung photons for section D than for section A which has almost the same wall shielding thickness ( $\text{g/cm}^2$ ). This inconsistency could be explained by the greater density of the ablation material (assuming higher atomic number materials) of wall section D (table I(b)). The more dense ablation material of section D produced more bremsstrahlung than the less dense ablation material of section A.

With 0.75 or 1.25 Mev electrons incident on the sections it can easily be seen that, as the detector angle increases from  $0^\circ$  to  $60^\circ$ , the bremsstrahlung intensity decreases. (See fig. 15.)

During three measurements on section C (figs. 12 and 13), with an electron energy of 1.25 Mev, the beam incidence angle was set at  $90^\circ$ ,  $60^\circ$ , and  $45^\circ$ . It can be seen from the figures that there is a decrease in bremsstrahlung intensity with a decrease in beam incidence angle. The significance of this decrease in bremsstrahlung intensity with an increase in detector angle or a decrease in beam incidence angle is that the emission of bremsstrahlung is in the direction of the incident electron beam.



## CONCLUSIONS

Measurements of the bremsstrahlung produced by 0.75 and 1.25 Mev electrons impinging upon typical Apollo wall sections were made during this investigation. Upon consideration of these measurements and the different typical Apollo wall sections, the following conclusions are presented:

1. The maximum dose rates are received through the wall section having the least shielding thickness ( $\text{g}/\text{cm}^2$ ).
2. The maximum dose rate and the bremsstrahlung photon intensity (counts/min) for all wall sections are always greatest in the direction of the electron beam and decrease sharply on each side of the beam.
3. The maximum bremsstrahlung photon intensity (counts/min) occurs at photon energies between 80 and 115 Kev for 0.75 and 1.25 Mev electrons.
4. For all wall sections there is a greater intensity of high-energy bremsstrahlung photons from incident 1.25 Mev electrons than from incident 0.75 Mev electrons.

Langley Research Center,  
National Aeronautics and Space Administration,  
Langley Station, Hampton, Va., July 24, 1964.

## REFERENCES

1. Foelsche, Trutz: Current Estimates of Radiation Doses in Space. NASA TN D-1267, 1962, pp. 1-12.
2. O'Brien, Brian J.: Radiation Belts. Sci. Am., vol. 208, no. 5, May 1963, pp. 84-96.
3. Allen, R. I.; Dessler, A. J.; Perkins, J. F.; and Price, H. C.: Shielding Problems in Manned Space Vehicles. NR-10<sup>4</sup> (Contract No. DA-01-009-506-ORD-832), Lockheed Nucl. Products (Marietta, Ga.), July 1960.
4. Evans, Robley D.: Principles for the Calculation of Radiation Dose Rates in Space Vehicles. Rep. No. 63270-05-01 (Contract NAS 5-664), Arthur D. Little, Inc., July 1961, pp. 45-83.
5. Anon.: Quarterly Radiation Shielding Status Report. SID 62-821-2, North Am. Aviation, Inc., Oct. 1962, pp. 47-76.
6. Jacobs, George J., ed. (With appendix A by J. R. Winckler): Proceedings of Conference on Radiation Problems in Manned Space Flight. NASA TN D-588, 1960.
7. Cleland, M. R.; and Morganstern, K. H.: A New High-Power Electron Accelerator. IRE, Trans. Ind. Electron., vol. IE-7, no. 2, July 1960, pp. 36-40.
8. Bell, P. R.: The Scintillation Method. Beta- and Gamma-Ray Spectroscopy, Kai Siegbahn, ed., Interscience Publ., Inc., 1955, pp. 133-164.
9. Vegors, Stanley H., Jr.; Marsden, Louis L.; and Heath, R. L.: Calculated Efficiencies of Cylindrical Radiation Detectors. AEC Res. and Dev. Rep. IDO-16370, U.S. At. Energy Comm., Sept. 1, 1958.
10. Heath, R. L.: Scintillation Spectrometry Gamma-Ray Spectrum Catalogue. AEC Res. and Dev. Rep. IDO-16408, U.S. At. Energy Comm., July 1, 1957.
11. Stanford, A. L., Jr.; and Rivers, W. K., Jr.: Efficiencies of Sodium Iodide Crystals. Rev. Sci. Instr., vol. 29, no. 5, May 1958, pp. 406-410.
12. Koch, H. W.; and Motz, J. W.: Bremsstrahlung Cross-Section Formulas and Related Data. Rev. Mod. Phys., vol. 31, no. 4, Oct. 1959, pp. 920-955.
13. Buechner, W. W.; Van de Graaff, R. J.; Burrill, E. A.; and Sperduto, A.: Thick-Target X-Ray Production in the Range From 1250 to 2350 Kilovolts. Phys. Rev., vol. 74, no. 10, Nov. 15, 1948, pp. 1348-1352.

14. Miller, William; Motz, J. W.; and Ciaella, Carmen: Thick Target Bremsstrahlung Spectra for 1.00-, 1.25-, and 1.40- Mev Electrons. Phys. Rev., vol. 96, no. 5, Dec. 1, 1954, pp. 1344-1350.
15. Ehrlich, Margarete: Scintillation Spectrometry of Low-Energy Bremsstrahlung. Res. Paper 2571, J. Res. Nat. Bur. Std., vol. 54, no. 2, Feb. 1955, pp. 107-118.

TABLE I.- PROPERTIES OF APOLLO WALL SECTIONS

(a) Composition of ablation materials

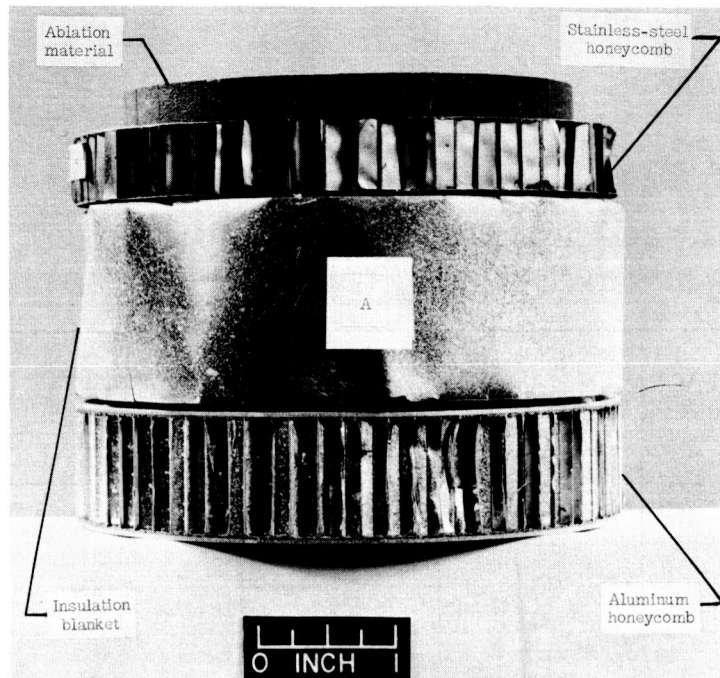
Element	Atomic number	Percent by weight for sections A, B, and C	Percent by weight for section D
Hydrogen	1	4.2	5.3
Carbon	6	54.2	60.1
Nitrogen	7	2.5	2.5
Oxygen	8	27.7	25.1
Silicon	14	11.4	7.0

(b) Physical properties

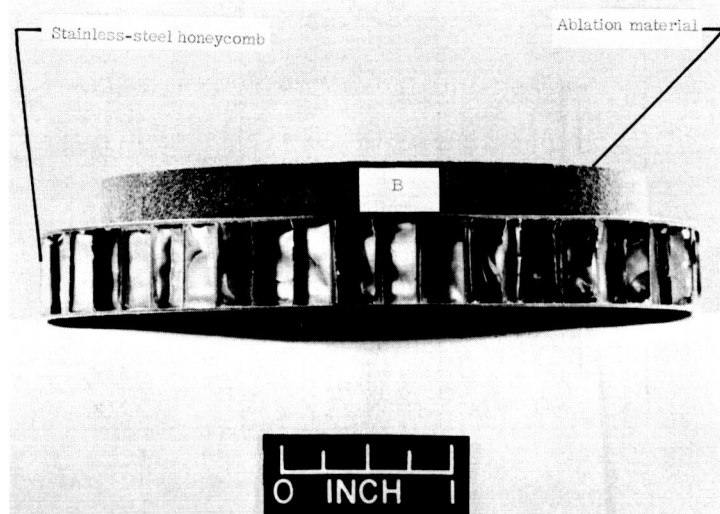
Wall component	Weight, g	Wall thickness, t, cm	Wall shielding thickness, pt, g/cm <sup>2</sup>	Faceplate thickness, cm	Measured density, ρ, g/cm <sup>3</sup>
Section A					
Ablator	51.5	0.945	0.565	----	0.595
Stainless-steel honeycomb	42.6	1.310	.468	0.02	-----
Insulation blanket	27.9	3.810	.366	----	.096
Aluminum honeycomb	67.6	2.380	.744	.08	-----
Total . . . . .	189.6	8.445	2.143		
Section B					
Ablator	45.4	0.945	0.497	----	0.524
Stainless-steel honeycomb	83.1	1.410	.914	0.05	-----
Total . . . . .	128.5	2.355	1.411		
Section C					
Ablator	222.2	3.81	2.440	----	0.637
Stainless-steel honeycomb	110.2	5.15	1.210	0.05	-----
Insulation blanket	17.0	2.03	.195	----	.096
Aluminum honeycomb	63.0	3.68	.690	.08	-----
Total . . . . .	412.4	14.67	4.535		
Section D					
Ablator	61.5	1.24	0.995	----	0.801
Stainless-steel honeycomb	42.6	1.31	.468	0.02	-----
Insulation blanket	22.1	2.03	.195	----	.096
Aluminum honeycomb	47.6	2.38	.523	.04	-----
Total . . . . .	173.8	6.96	2.181		

TABLE II.- DOSE RATES FOR APOLLO WALL SECTIONS

Section	Detector angle, deg	Beam incidence angle, deg	Electron energy, Mev	Normalized beam current, nA	Normalized dose rate, mR/hr
A	0	90	1.25	100	176.3
A	15	90	1.25	100	130.3
A	0	90	.75	100	32.6
A	15	90	.75	100	27.4
B	0	90	1.25	100	185.8
B	15	90	1.25	100	138.8
B	0	90	.75	100	34.3
B	15	90	.75	100	27.0
C	0	90	1.25	100	146.5
C	15	90	1.25	100	105.3
C	0	90	.75	100	30.4
C	15	90	.75	100	21.6
C	30	60	1.25	100	71.3
C	45	45	1.25	100	45.1
D	0	90	1.25	100	154.7
D	15	90	1.25	100	109.6
D	30	90	1.25	100	66.0
D	45	90	1.25	100	40.0
D	60	90	1.25	100	21.0
D	0	90	.75	100	30.6
D	15	90	.75	100	25.4



(a) Wall section A.

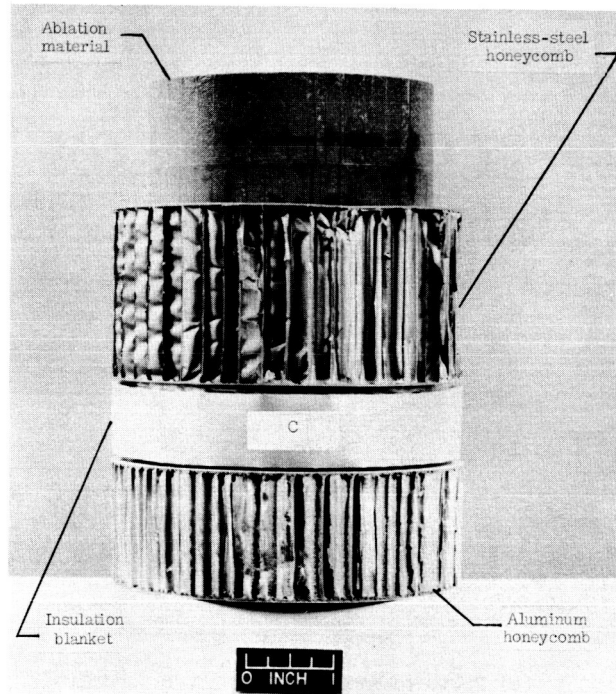


(b) Wall section B.

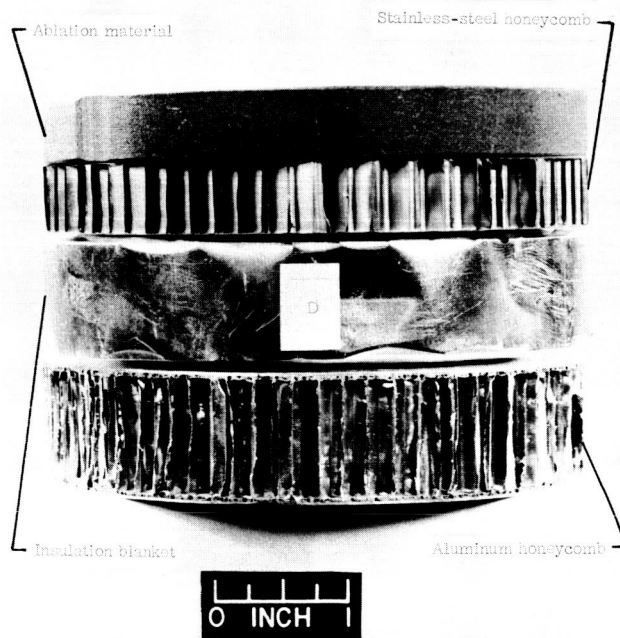
L-64-4748

Figure 1.- Apollo wall sections used in the investigation.





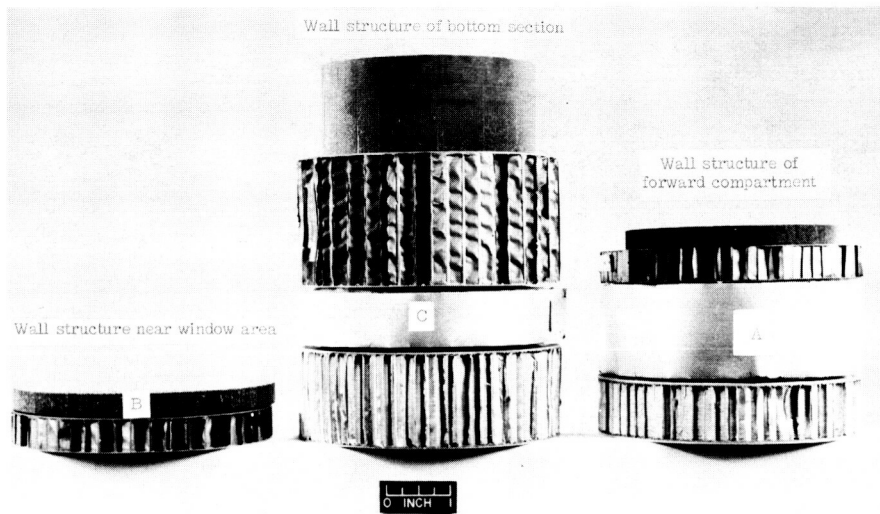
(c) Wall section C.



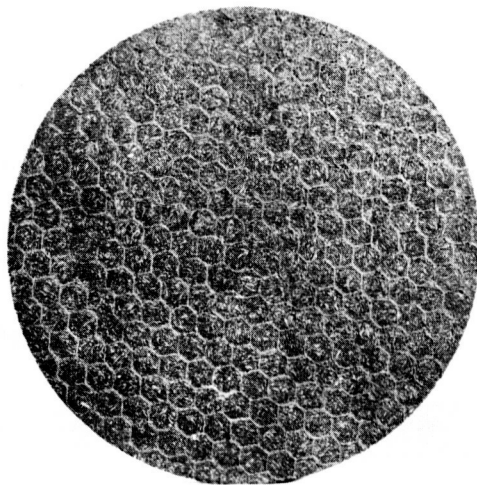
(d) Wall section D.

L-64-4749

Figure 1.- Continued.



(e) Parts of wall sections A, B, and C.



(f) End section of honeycomb ablation material. L-64-4750

Figure 1.- Concluded.

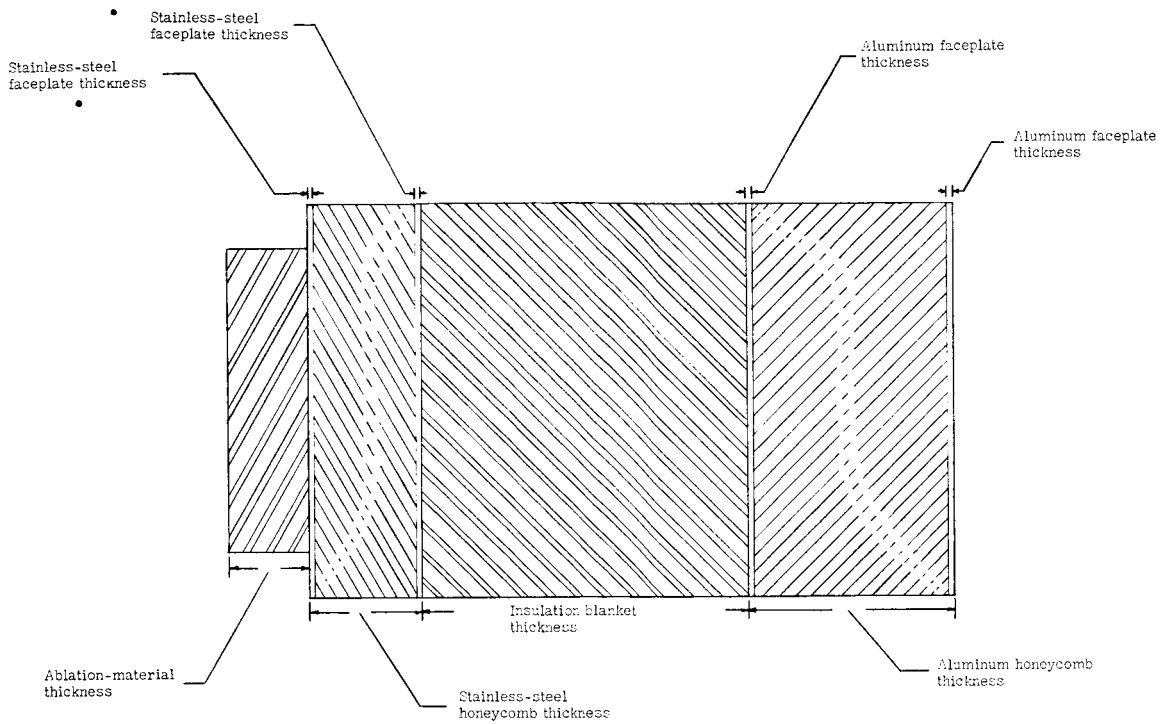


Figure 2.- Details of Apollo wall section.

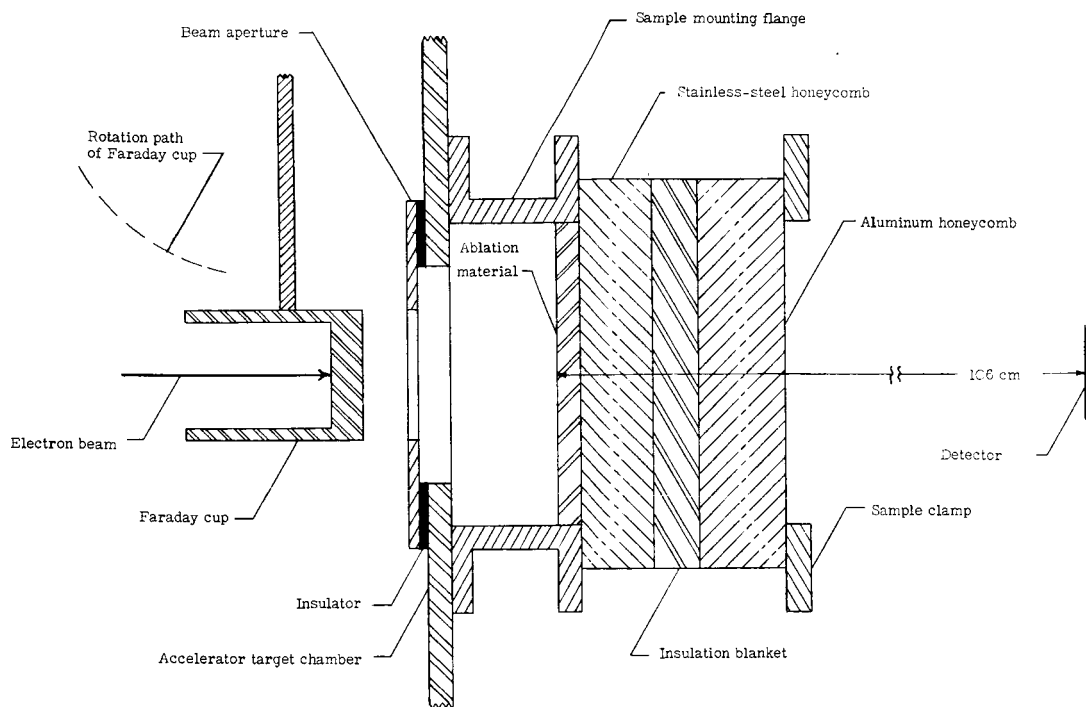


Figure 3.- Side view of Apollo wall-section mounting details and Faraday cup.

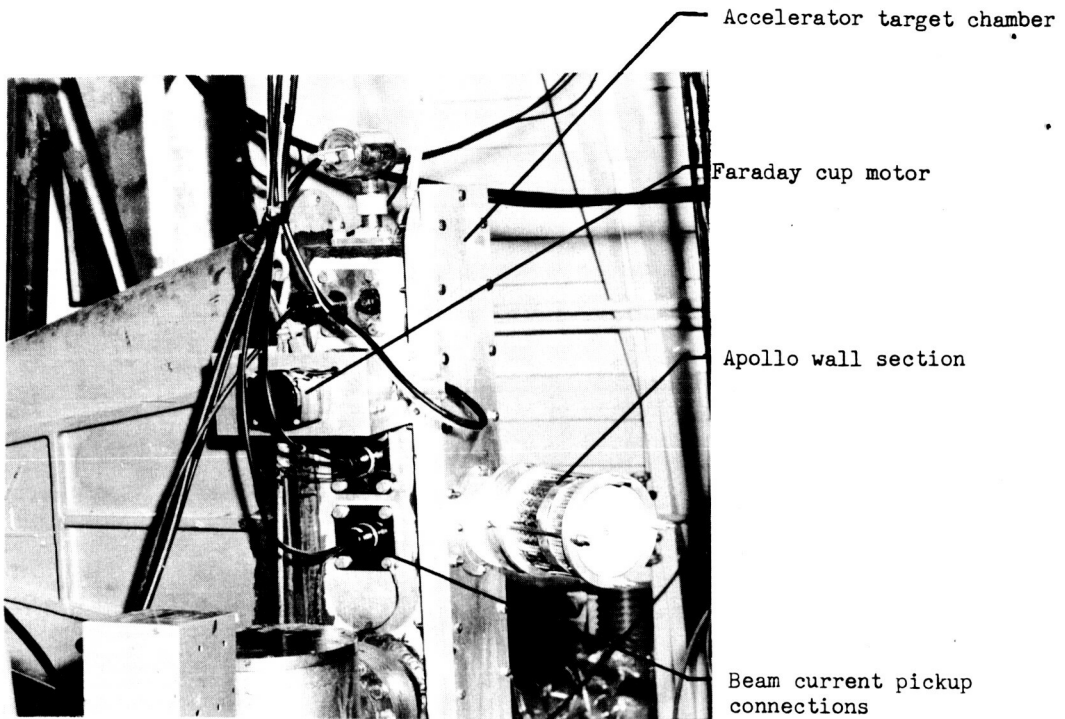


Figure 4.- Accelerator target chamber with Apollo wall section C mounted at a beam incidence angle of  $45^\circ$ . L-63-5379.1

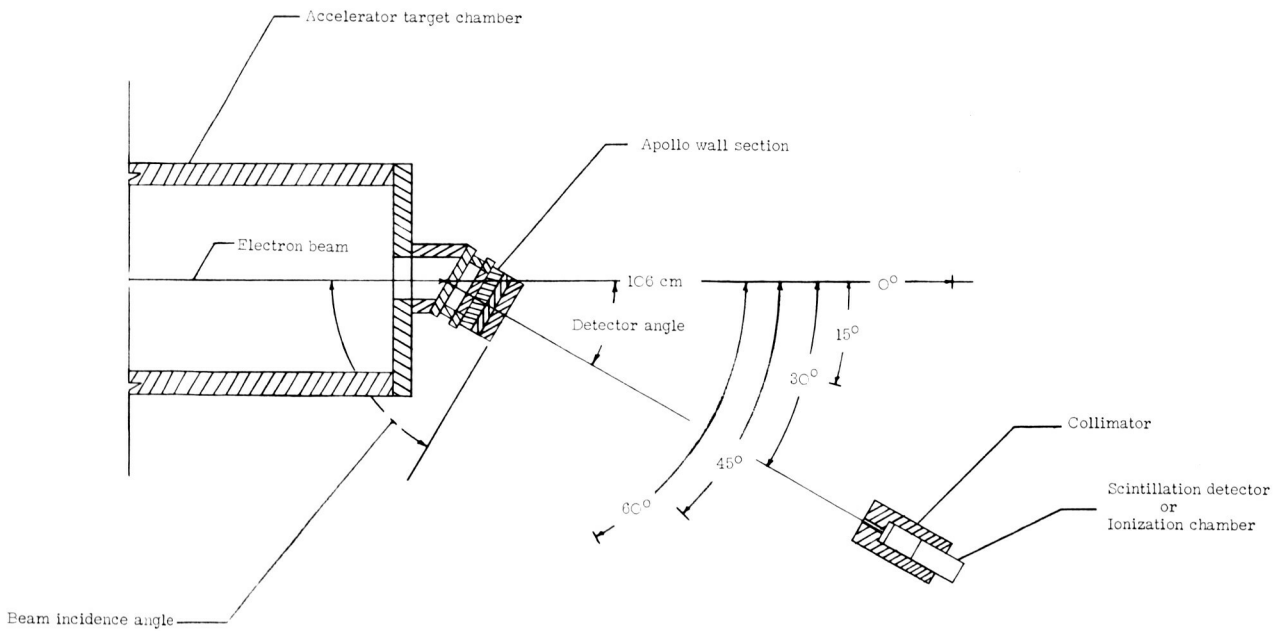


Figure 5.- Top view of position of scintillation detector or ionization chamber relative to Apollo wall section during measurements.

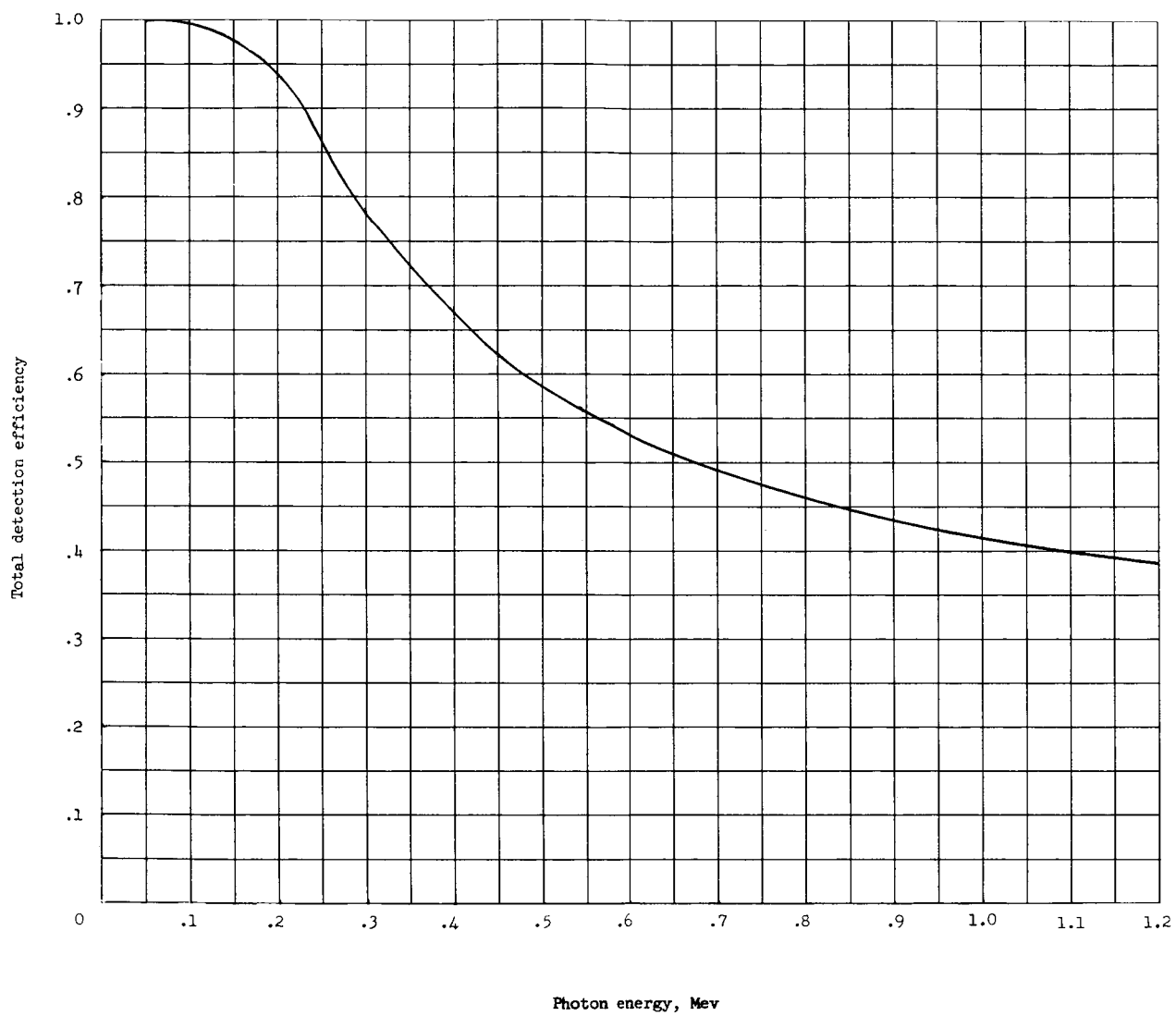
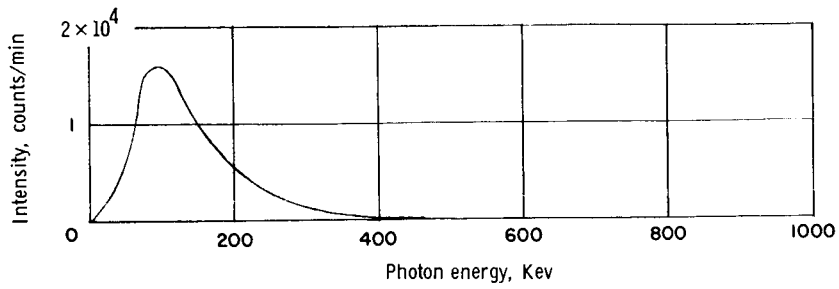
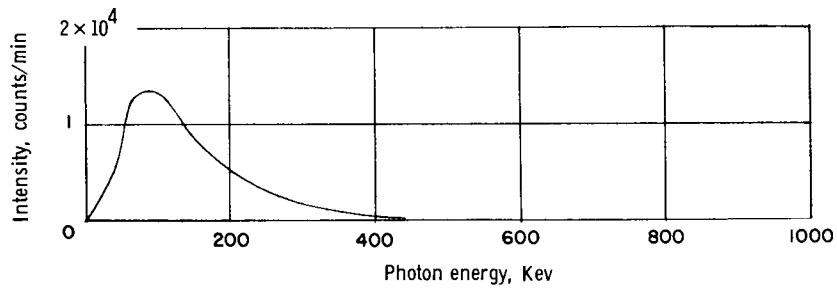


Figure 6.- Total detection efficiency curve for  $1\frac{1}{4}$ -inch by 1-inch NaI(Tl) scintillation detector.



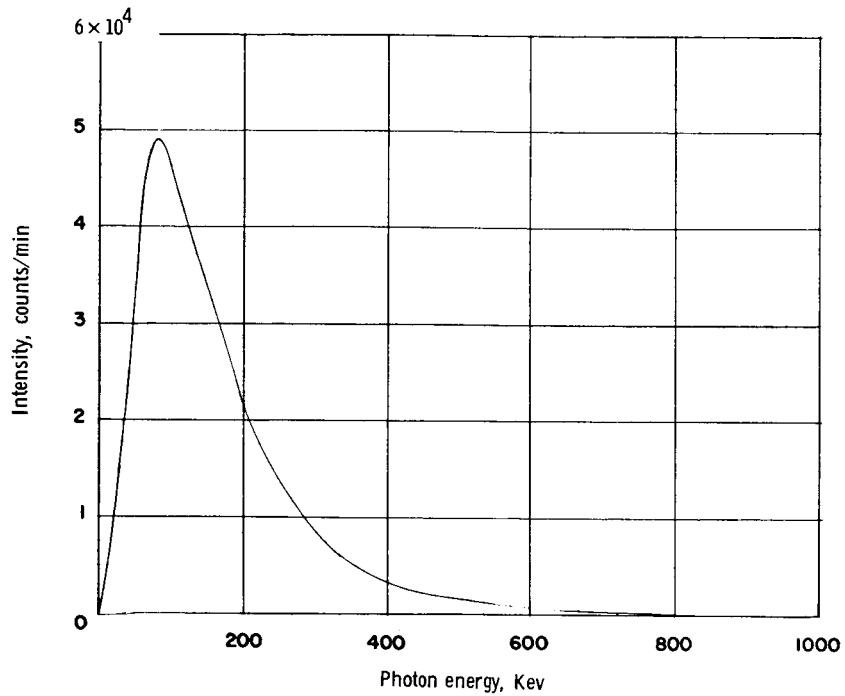
(a) Detector angle,  $0^\circ$ .



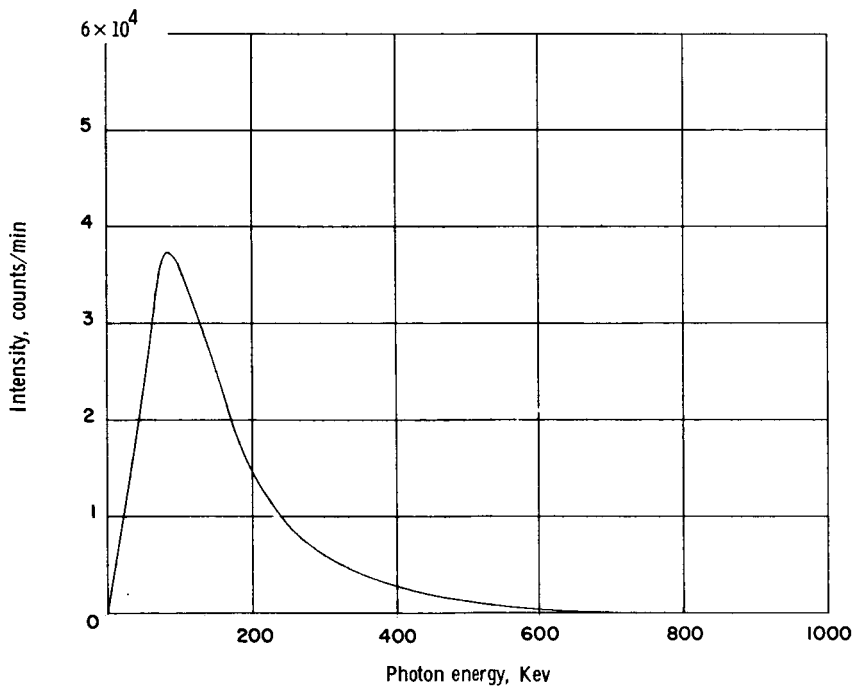
(b) Detector angle,  $15^\circ$ .

Figure 7.- Bremsstrahlung spectra from wall section A. Electron energy, 0.75 Mev; beam incidence angle,  $90^\circ$ .



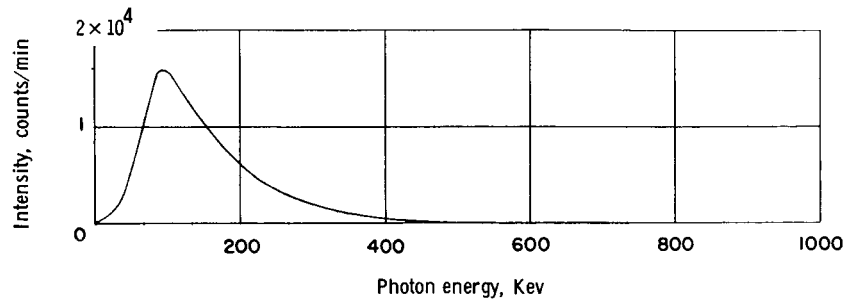


(a) Detector angle,  $0^\circ$ .

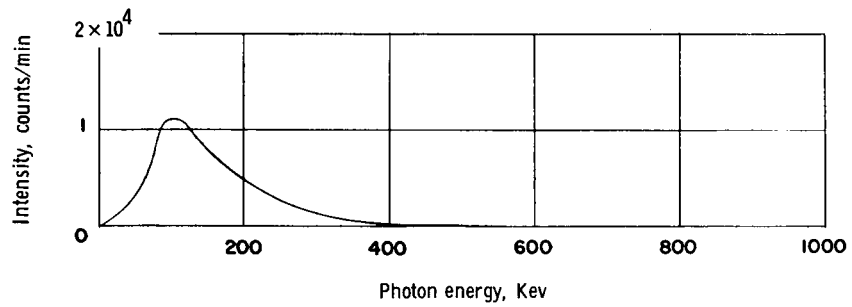


(b) Detector angle,  $15^\circ$ .

Figure 8.- Bremsstrahlung spectra from wall section A. Electron energy, 1.25 Mev; beam incidence angle,  $90^\circ$ .

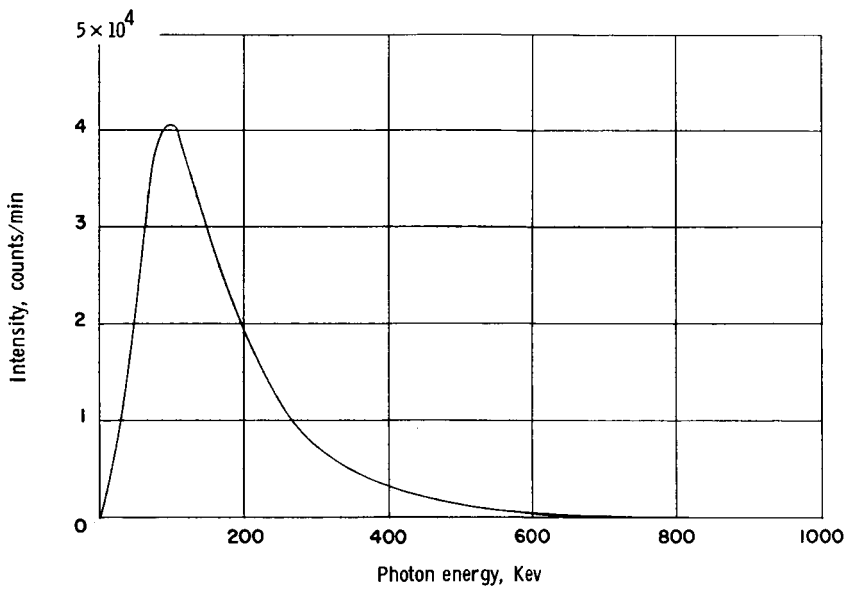


(a) Detector angle,  $0^\circ$ .

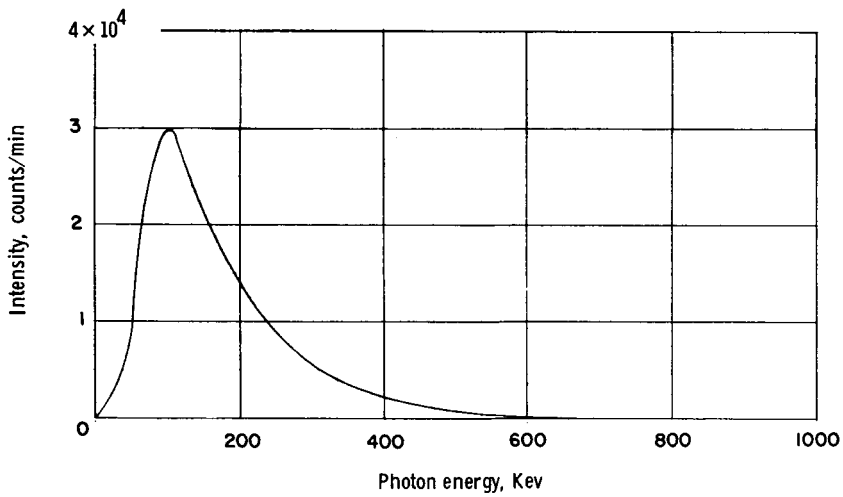


(b) Detector angle,  $15^\circ$ .

Figure 9.- Bremsstrahlung spectra from wall section B. Electron energy, 0.75 Mev; beam incidence angle,  $90^\circ$ .

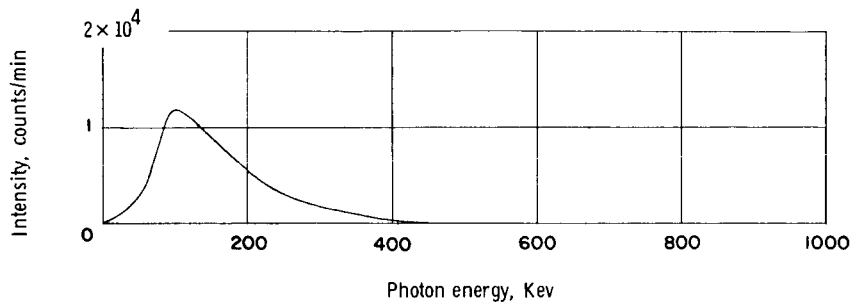


(a) Detector angle,  $0^\circ$ .

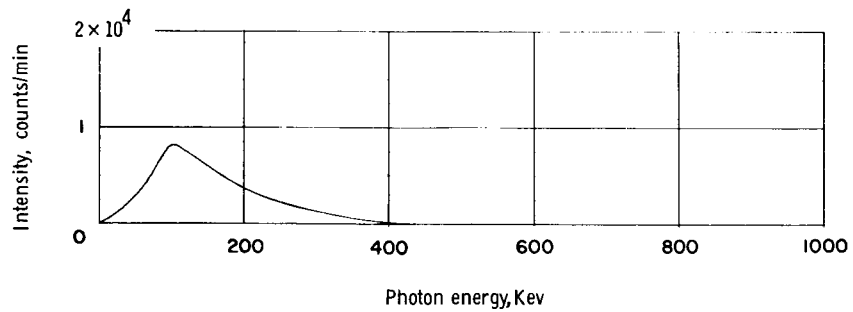


(b) Detector angle,  $15^\circ$ .

Figure 10.- Bremsstrahlung spectra from wall section B. Electron energy, 1.25 Mev; beam incidence angle,  $90^\circ$ .

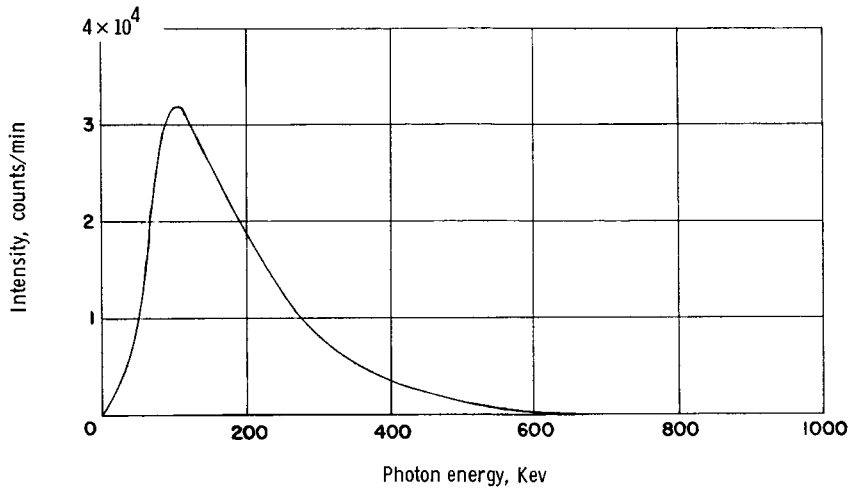


(a) Detector angle,  $0^\circ$ .

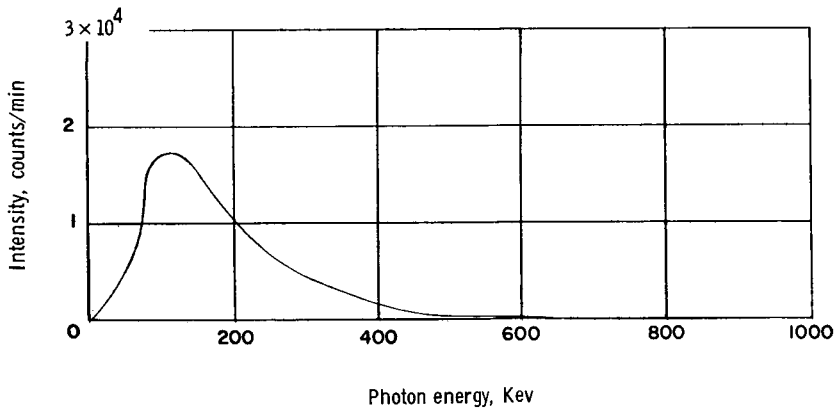


(b) Detector angle,  $15^\circ$ .

Figure 11.- Bremsstrahlung spectra from wall section C. Electron energy, 0.75 Mev; beam incidence angle,  $90^\circ$ .

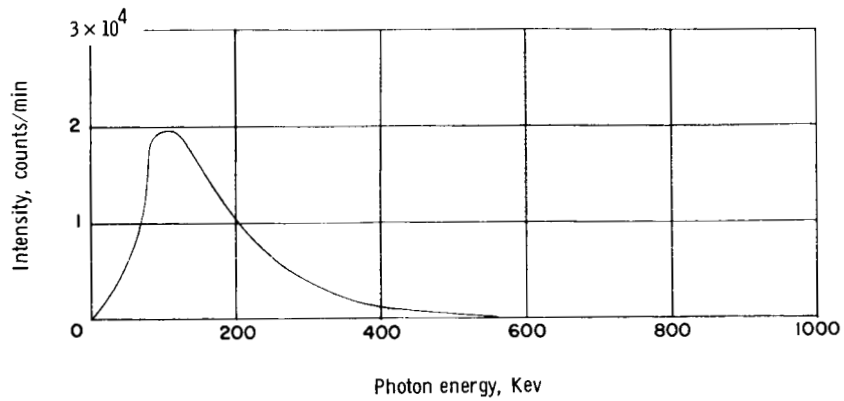


(a) Detector angle,  $0^\circ$ .

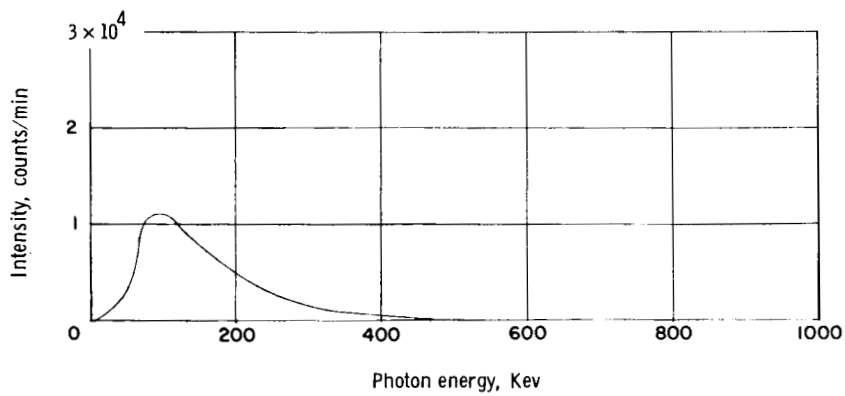


(b) Detector angle,  $15^\circ$ .

Figure 12.- Bremsstrahlung spectra from wall section C. Electron energy, 1.25 Mev; beam incidence angle,  $90^\circ$ .



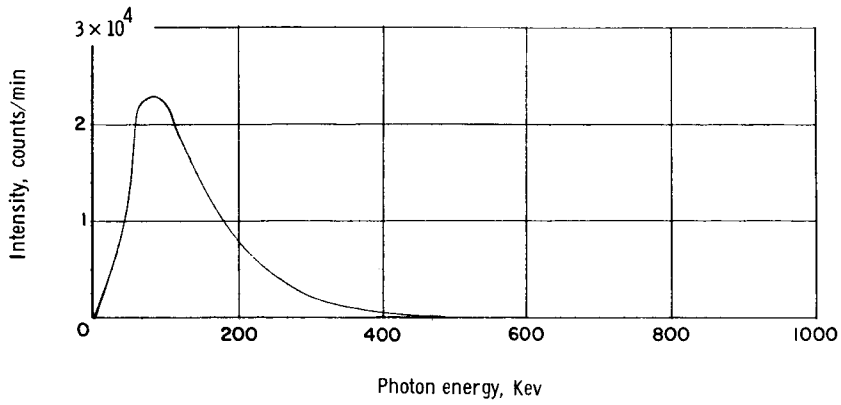
(a) Beam incidence angle,  $60^\circ$ ; detector angle,  $30^\circ$ .



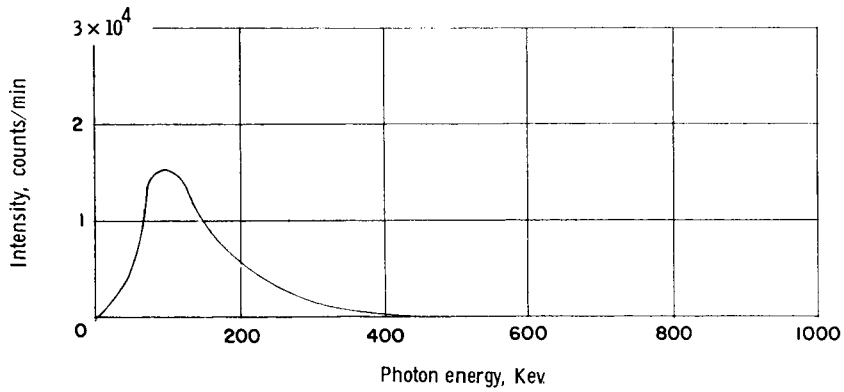
(b) Beam incidence angle,  $45^\circ$ ; detector angle,  $45^\circ$ .

Figure 13.- Bremsstrahlung spectra from wall section C. Electron energy, 1.25 Mev.



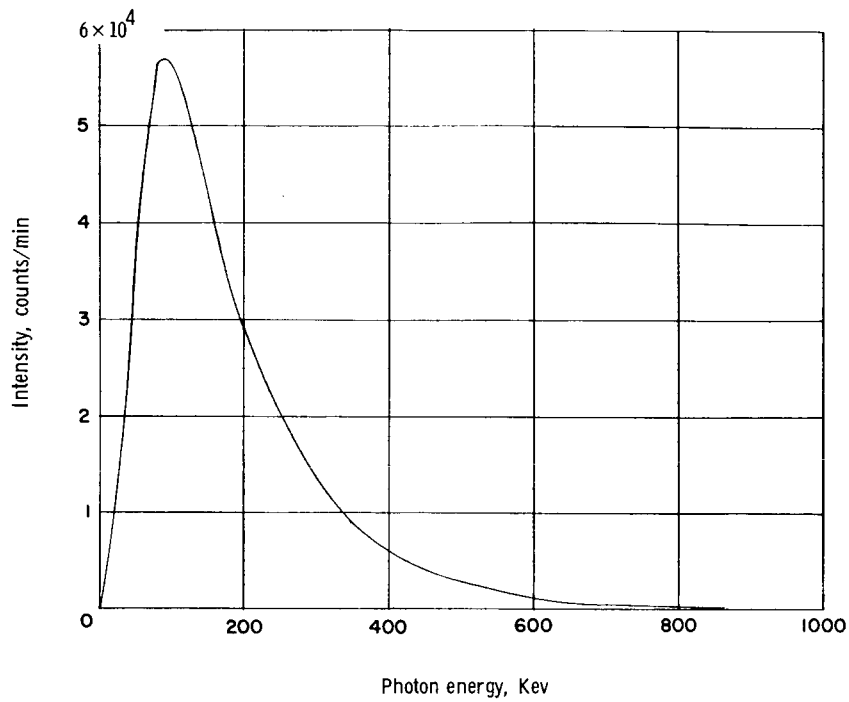


(a) Detector angle,  $0^\circ$ .

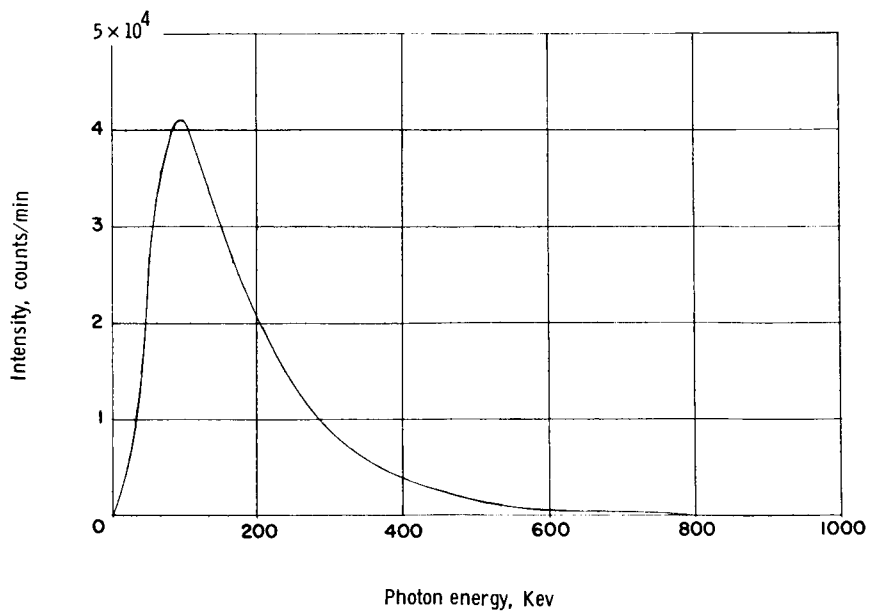


(b) Detector angle,  $15^\circ$ .

Figure 14.- Bremsstrahlung spectra from wall section D. Electron energy, 0.75 Mev; beam incidence angle,  $90^\circ$ .

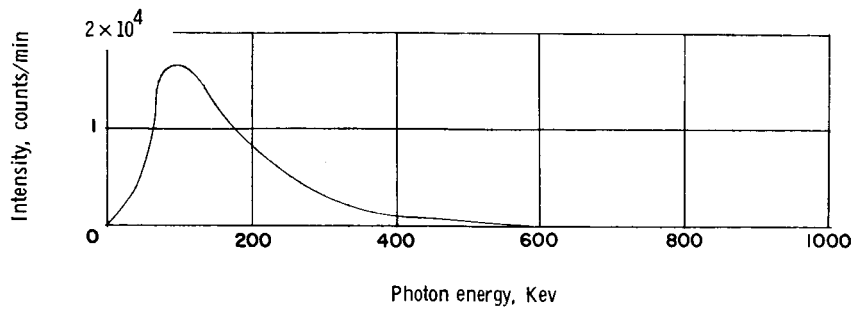


(a) Detector angle,  $0^\circ$ .

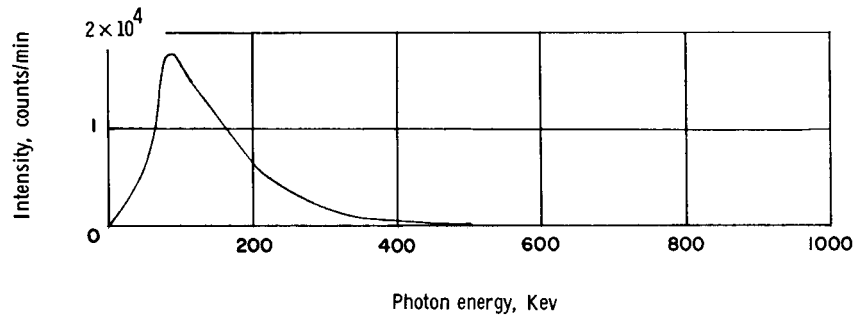


(b) Detector angle,  $15^\circ$ .

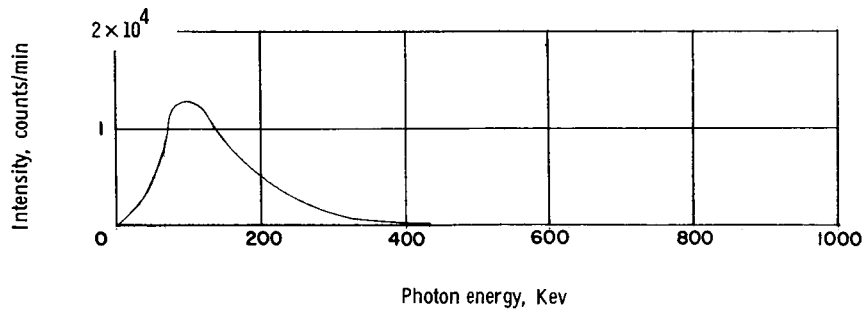
Figure 15.- Bremsstrahlung spectra from wall section D. Electron energy, 1.25 Mev; beam incidence angle,  $90^\circ$ .



(c) Detector angle,  $30^\circ$ .



(d) Detector angle,  $45^\circ$ .



(e) Detector angle,  $60^\circ$ .

Figure 15.- Concluded.